Electrostatically driven and capacitively detected differential lateral resonant pressure microsensor

Hailong Jiao[1,2], Bo Xie[1,2], Junbo Wang[1], Deyong Chen[1], Jian Chen[1]

[1]*State Key Laboratory of Transducer Technology, Institute of Electronics, Chinese Academy of Sciences, Beijing 100190, People's Republic of China*
[2]*College of Electrical and Communication Engineering, University of Chinese Academy of Sciences, Beijing, 100080, People's Republic of China*
E-mail: jbwang@mail.ie.ac.cn

Published in Micro & Nano Letters; Received on 13th May 2013; Revised on 8th August 2013; Accepted on 5th September 2013

Presented is the design, fabrication and characterisation of an electrostatic-driving and capacitive-detection differential resonant pressure microsensor. The differential structure consists of two resonators immobilised on the diaphragm. In response to the pressure under measurement, the diaphragm deflection increases the intrinsic resonant frequency of one resonant beam and decreases the resonant frequency of the other. A differential frequency output reduces the common frequency drift caused by stresses and interferences, and thus improves the sensor's stability. The device geometries were optimised using numerical simulations and the fabrication process was based on a silicon-on-insulator wafer requiring only two masks with simplified microfabrication steps (e.g. sputter, wet etching and deep reactive ion etching). The sensor was quantified in an open-loop characterisation platform, producing a quality factor higher than 10 430 in vacuum (< 0.5 Pa). Closed-loop test results recorded a linear resonant frequency shift (a linear correlation of 0.9999) in response to applied pressure, with a sensitivity of 227 Hz/kPa. This resonant pressure microsensor has a simple fabrication process and reliable performance, and can be used for pressure monitoring in various locations including weather stations and aerospace.

1. Introduction: Silicon resonant pressure microsensors have been widely used in the automotive industry, and in the medical instrument, aerospace and military fields because of their high sensitivity, high linearity, long-term stability and quasi-digital output [1–3]. Methods to drive resonators are based on thermal [4], piezoelectric [5], electrostatic [6] or electromagnetic [3, 7] forces whereas vibrations can be detected using piezoresistive [6], electromagnetic [3] or capacitive principles [8].

Among all the approaches, resonators with electrostatic excitation and capacitive detection are featured with reliable performance because of low current, low thermal noises and low power consumption [8–10]. However, previously reported microsensors [2, 5] have complex structures, requiring complicated fabrication processes. In addition, a metal layer is always needed for electrical wire connection, leading to the problem of residual stress because of thermal coefficient mismatch between metal and silicon [11].

To address these issues, a new lateral resonant pressure microsensor based on the electrostatic-driving and capacitive-detection principle is proposed in this Letter, where the residual stress is minimised since a highly doped silicon layer with low resistance rather than a metal layer is used for electrical connections. In addition, the fabrication processes were significantly simplified by using silicon-on-insulator (SOI) wafers where only two masks were required for device fabrication. Furthermore, a differential design capable of producing a differential frequency output was also used in this study, aimed at reducing the resonant frequency drift caused by residual stress or temperature variations.

2. Methodology

2.1. Working mechanism: As shown in Fig. 1, the device is constructed from an SOI wafer, including three functional layers, namely the substrate layer, the SiO_2 sacrificed layer and the device layer. The substrate layer is made of a 100 μm silicon-based diaphragm, to sense pressure under measurement. The device layer, made of a 40 μm-thick heavily doped silicon layer (0.001–0.002 Ω cm), forms the resonators, conductive tracks and pads, which are electrically isolated from the substrate layer by SiO_2.

To decrease the side-effect of temperature on resonant frequency output, a differential design was used in this study where two silicon resonators were organised along the diagonal direction (horizontal direction, <100>) suspended on the silicon square diaphragm. The resonant beam located near the centre of the diaphragm is named the 'middle beam' and the other one is named the 'sidewall beam'. Both resonant beams have the same dimensions (length: 1600 μm, width: 20 μm, thickness: 40 μm), and thus the same intrinsic resonant frequency at zero pressure. Each resonator consists of a clamped–clamped beam and two parallel plates, forming driving and detecting capacitors, respectively, with a gap of 5 μm between the beam and the plate.

When pressure under measurement is applied on the diaphragm, the diaphragm deflection induces a tensile stress in the middle beam with an increase in the resonant frequency whereas the sidewall beam is under a compressive stress with a resonant frequency decrease. The output frequency difference between these two resonant beams reflects the amplitude of pressure under measurement. In response to thermal residual stress or material characteristic drifts because of the temperature variation, the resonant frequencies of the two resonators drift in the same direction, which can partially reduce the drifts based on the differential setup.

2.2. Design optimisation: Mode interference and sensitivity mismatch are two key factors in device design and optimisation. Mode interference or the resonant frequency overlap of two nearby modes can drive the resonant sensor to vibrate in undesirable modes, leading to a decrease in quality factor. Sensitivity mismatch between the middle and the sidewall beams can lead to compromised performance in the differential resonant frequency output.

In this study, numerical simulations based on finite element analysis (FEA) were used to optimise the design of the microsensor. Static simulations were used to calculate the stress distribution along the resonant microbeams as a function of pressure. Then, mode simulations were conducted to transfer resonant beam stresses into the intrinsic resonant frequency shift.

© The Institution of Engineering and Technology 2013

doi: 10.1049/mnl.2013.0271

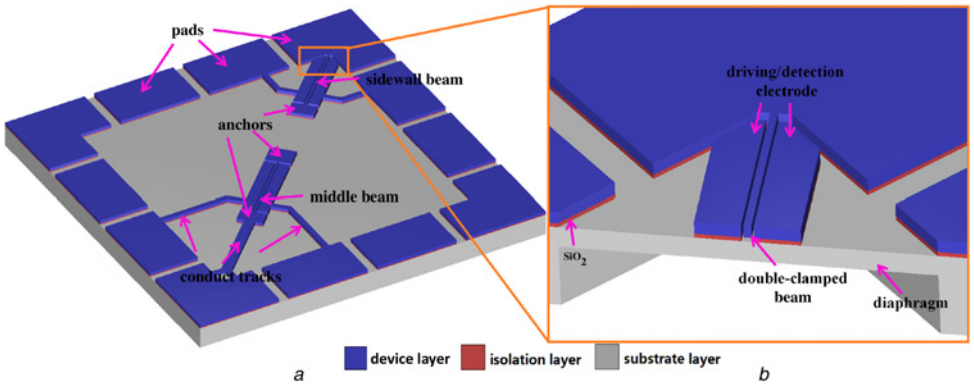


Figure 1 *Schematic of proposed device including three functional layers, namely the substrate layer, sacrificed layer and device layer*
a The substrate layer contains a 100 μm silicon-based square diaphragm used to sense pressure under measurement. The device layer, 40 μm-thick heavily doped silicon layer, forms the resonators, which are electrically isolated from the substrate layer by the 2 μm SiO_2 sacrificed layer. Each resonator was composed of a driving/detection electrode and double-end-clamped beam fixed on the diaphragm by two anchors
b The zoom in for the key portion and cross section of Fig. 1*a*

More specifically, static simulations based on the ANSYS@11.0 software platform were conducted as follows. The element type 'Solid 10-node 92' was used to mesh the prototype of the microsensor for both static structural and mode analysis with the detailed material properties shown in Table 1. A meshing with the element size of 20 μm was used to mesh the substrate layer and the pads. As for smaller structures like the isolation layer, anchors and the beams, an element size of 5 μm was used. The boundary area of the pressure sensitive diaphragm was completely restrained in all the degrees of freedom without any freedom to prevent unconstrained movement. A series of pressures with values of 0, 0.025, 0.05, 0.075 and 0.1 MPa were applied on the backside of the diaphragm, respectively.

Following the static simulations, mode simulations were implemented by extracting all the modes within the frequency ranging from 0 to 100 kHz. Furthermore, simulations were used to investigate the position effect on the resonant frequencies of the middle beam and the sidewall beam, which aimed to achieve identical sensitivities. Detailed device parameters are shown in Table 1, which were derived from the previous experimental parameters [3].

2.3. Fabrication and packaging: The starting material was a 4 inch SOI wafer with a 40 μm <100> device layer, a 2 μm-thick SiO_2 sacrificed layer and a 300 μm-thick <100> substrate layer. The first step of device fabrication was to form a 100 μm diaphragm on the substrate layer through photoresist lithography and wafer dry etching, shown in Figs. 2*a–d*. Photoresist lithography included AZ4620 photoresist spin-coating on the substrate layer (1000 rpm for 60 s), soft-bake (45 min at 80°C), exposure to ultraviolet (UV) light (26 s, 15 mW/cm^2) through a chrome-on-glass mask, development (Developer AZ300) and hard-bake (1 h at 120°C). Then, the patterned photoresist was used as the mask of deep reactive ion etching (DRIE) to remove 200 μm of the substrate, forming the diaphragm.

The second step was to fabricate the resonant beams in the structure layer (see Figs. 2*e–k*). To guarantee the verticality of the 5 μm gap between the driving/detection plate and the doubly clamped beam, a 200 nm aluminium film was sputtered on the top layer of the wafer as the etching mask. Following AZ1500 photoresist spin-coating (1000 rpm for 60 s) and soft-bake (40 min at 80°C), the photoresist was exposed to UV light (3.8 s, 15 mW/cm^2) using the second chrome-on-glass mask, and then developed with AZ300 for 135 s. The wafer with patterned photoresist was then soaked in H_3PO_4 to remove the exposed aluminium. The wafer was immediately removed from the H_3PO_4 solution to avoid over-etch laterally when the exposed aluminium was totally etched. Then, the device layer was etched by DRIE to reach the sacrificed layer with the mask layers removed.

Table 1 Parameter list used in FEA simulation

Items	Parameters	Values	Units
silicon	Young's modulus	165	GPa
	density	2.3	g/cm^3
	Poisson's ratio	0.24	
beams	length	1600	μm
	width	20	μm
	thickness	40	μm
diaphragm	length and width	5200	μm
	thickness	100	μm
sensor chip	length and width	6800	μm
	thickness	342	μm

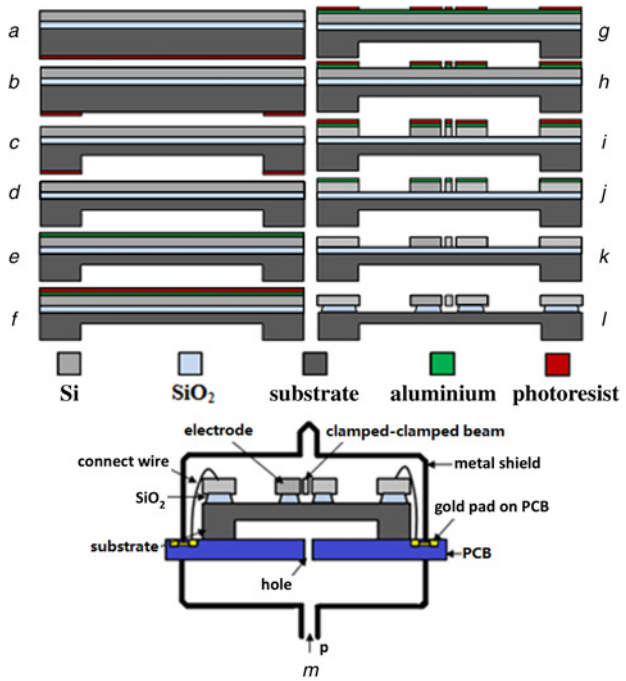


Figure 2 *Device fabrication process and packaging*
a–d Diaphragm fabrication
e–i Resonant beam fabrication and release
j–l Wafer cleaning and moveable structure release
m Device packaging

© The Institution of Engineering and Technology 2013

The last step was to release the resonators by removing the sacrificed layer using the hydrofluoric acid (HF) buffer solution ($HF : NH_4F : H_2O = 3 : 6 : 10$, in volume), followed by immersion in isopropyl alcohol to avoid strictness [12].

The sensor packaging is shown in Fig. 2*m*, where the microchip was packaged with a printed circuit board using the epoxy structural adhesive of WD3620. Then, the wire connected resonators were sealed in a metal shield with the diaphragm used to sense pressure under measurement exposed to the atmosphere by means of an air hole in the metal shield.

2.4. Experimental setup: The sensor was first characterised by an open-loop system, using the network analyser E5061B (Agilent, USA), shown in Fig. 3*a*. The driving principle was as follows. The detection plate was grounded virtually using an operational amplifier whereas the resonant beam was applied with a DC bias. By applying a small sinusoidal signal on the driving plate, the resonant beam was driven to vibrate by two unbalanced electrostatic forces from the electrodes, leading to capacity change as the output. In our experiment, a DC bias voltage of 30 V was applied on the resonant beam and a sinusoidal excitation signal of 3.98 mV was applied to the excitation plate. The substrate layer was electrically grounded to decrease the co-channel interference resulting from the capacitive crosstalk. Under beam vibration, the change of the detection capacitor was translated to a voltage output by a charge amplifier circuit.

A closed-loop system was developed to detect the resonant frequency of the resonant pressure microsensor. Fig. 3*b* shows the schematic diagram of the system, where a reference resonator without the DC bias was used to compensate for the crosstalk caused by the parasitic capacitors between the driving and detection electrodes. The common noise signal was reduced, and the vibration signal was amplified by an instrument amplifier. Then, automatic gain control (AGC) circuits, consisting of a bandwidth filter, a rectifier, an error detector and a junction transistor, were used to control the oscillation amplitude of the microbeam.

The device was quantified in a confined chamber where the pressure was finely tuned by a pressure calibrator (DPI 610, Druck, UK). The output period voltage signals of the two resonant beams were translated into frequency outputs at the same time. Thus, the differential frequency was calculated by the frequency output difference of the two beams.

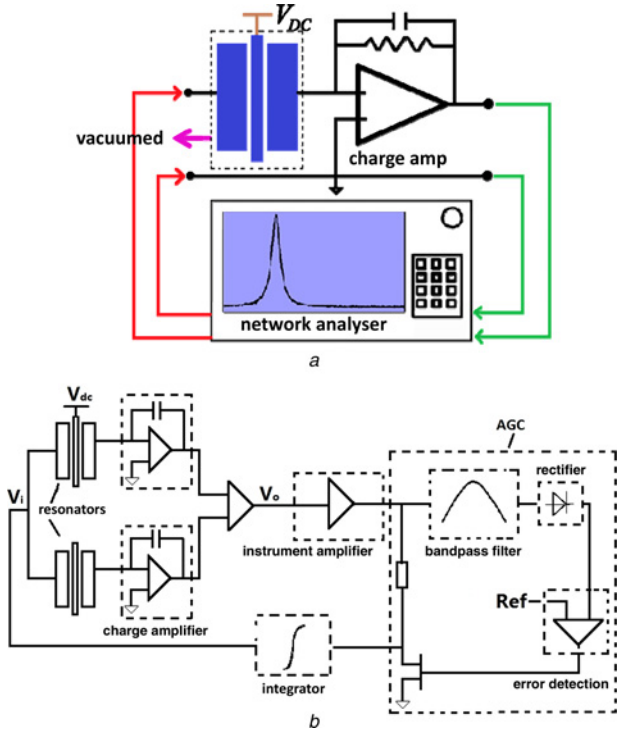


Figure 3 *Open-loop characterising circuit (Fig. 3a) for resonant frequency detection where charge amplifier was used to translate output charge signals into voltage signals, monitored by a network analyser; self-oscillation system (Fig. 3b) with additional reference resonator used to decrease voltage crosstalk and improve signal-to-noise ratio of preamplifier*
AGC system was used to ensure constant amplitude vibration of the microsensor

3. Results and discussion

3.1. Simulation results: The simulation results recorded three resonant modes within 100 kHz, which may have side-effects on the specific resonant mode used in this study because of the vibration crosstalk (see Fig. 4). Mode 1 represents the

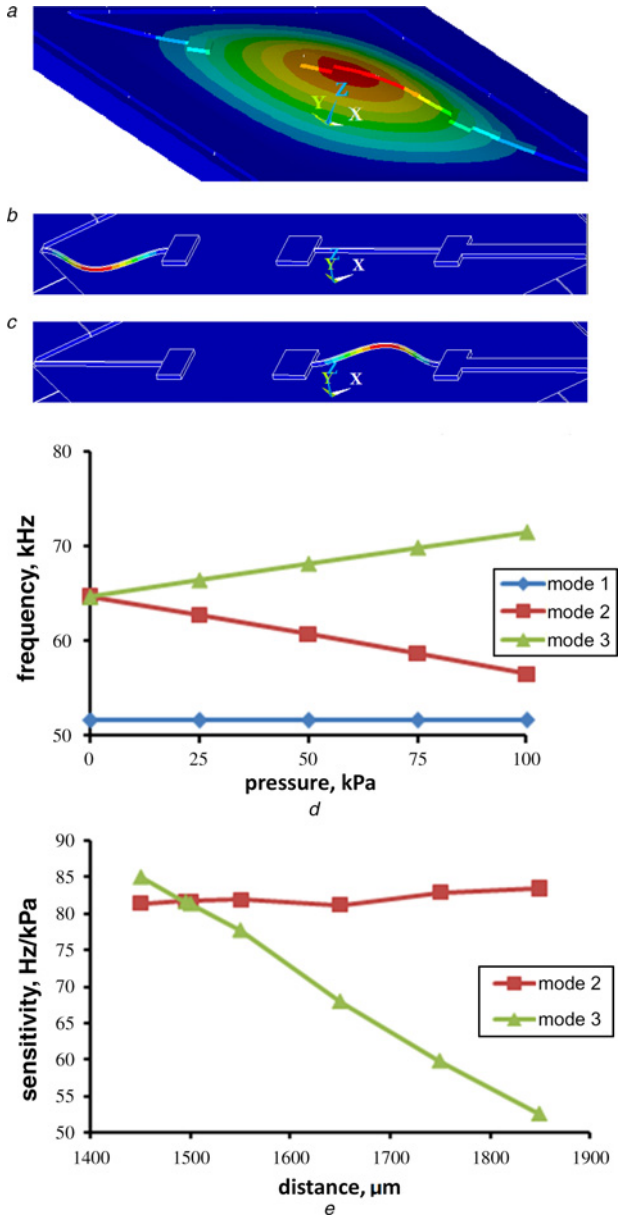


Figure 4 *Numerical simulation results*
a Out-of-plane vibrations, interfered with by diaphragm oscillation
b and *c* Maximal displacement of middle beam and sidewall beam in first-order lateral resonance vibration modes
d Resonant frequencies of beams and diaphragm modulated by pressure under measurement
e The effect of distance between middle and sidewall beam on device output sensitivity

© The Institution of Engineering and Technology 2013

doi: 10.1049/mnl.2013.0271

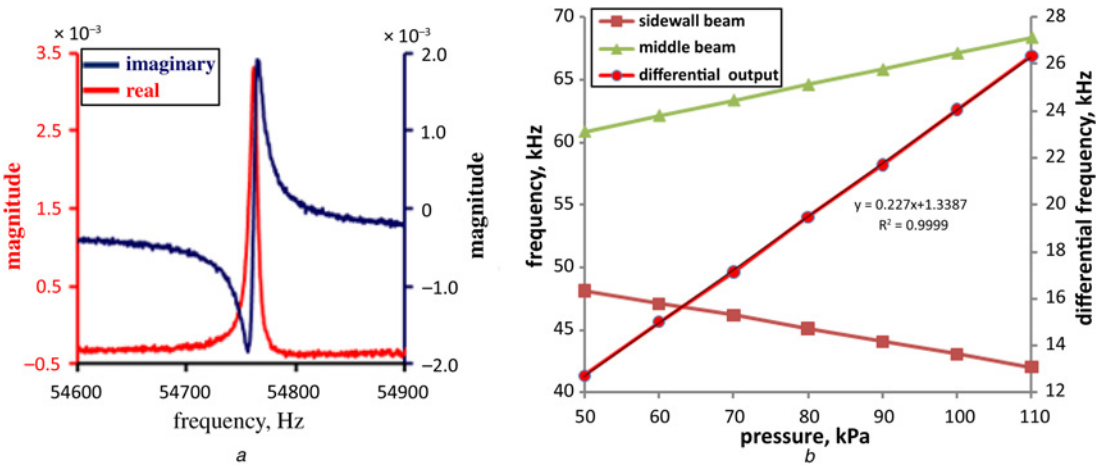


Figure 5 *Frequency sweeping result of sidewall beam at 0 Pa, locating a resonant frequency of 54 762 Hz with amplitude peak in real part and sharp change in imaginary part (Fig. 5a); the y-axis represents the ratio of amplitude of output-to-input voltage V_o/V_i, in the domain of real and imagine, respectively. Resonant frequency output against applied pressure (Fig. 5b); the two beams have small sensitivities which reduce the effect of small residual stress, but a doubled sensitivity of 227 Hz/kPa is enough for employment by a differential output*

out-of-plane oscillation of the diaphragm clamped with the resonant beams. Modes 2 and 3 represent the lateral vibration of the sidewall and the middle beam, respectively, as shown in Figs. 4*b* and *c*. Fig. 4*d* shows that the resonant frequency of the diaphragm was much lower than the intrinsic frequencies of the resonant beams, confirming that there is no concern relating to the issue of mode vibration crosstalk.

The sensitivities of both resonant beams based on numerical simulations were plotted against distance between these two resonant beams. As shown in Fig. 4*e*, an optimised distance of 1500 µm between these two microbeams was chosen to produce a comparable frequency shift in response to pressure under measurement with a sensitivity of roughly 162 Hz/kPa.

3.2. Characterisation results: The performance of the resonant pressure microsensor is shown in Fig. 5*a*, recording the middle beam resonant frequency of 54 762 Hz (quality factor of 10 430) and the sidewall resonant frequency of 53 258 Hz (quality factor of 10 523) in vacuum. When the resonant beams are excited by a high AC voltage, there is a concern of nonlinearity [13]. Thus, the AC driving voltage used in this study for the closed-loop measurement was < 50 mV. A linear differential frequency shift was located in response to applied pressure, which is shown in Fig. 5*b*. The calculated device sensitivity was 227 Hz/kPa in the pressure range of 50–110 kPa, with a linear correlation of 0.9999. The sensitivity quantified was higher than that of the simulation because of the undercut etching during the process of resonator release in HF, decreasing the sizes of the anchors, which softened the diaphragm.

4. Conclusion: An electrostatic-driving and capacitive-detection differential lateral resonant pressure sensor using an SOI wafer is demonstrated in this Letter. Based on the two-mask fabrication process, heavily doped silicon was successfully used to replace metal materials for electrical connection. The measurement results confirmed that the sensor was capable of producing a quality factor >10 430, producing a linear differential frequency shift with a correlation of 0.9999 in response to applied pressure. Device sensitivity was quantified as 227 Hz/kPa in the pressure range of 50–110 kPa.

5. Acknowledgments: This work is supported by the Beijing Municipal Science and Technology Commission (China) with project no. D11110100160000 and the NSFC (National Natural Science Foundation of China) with project no. 61072022.

6 References

[1] Beeby S., Ensell G., Kraft M., White N.: 'MEMS mechanical sensors' (Artech House, Boston, MA/London, 2004)
[2] Kinnell P.K., Craddock R.: 'Advances in silicon resonant pressure transducers', *Procedia Chem. I*, 2009, **1**, pp. 104–107
[3] Chen D., Li Y., Liu M., Wang J.: 'Design and experiment of a laterally driven micromachined resonant pressure sensor for barometers', *Procedia Eng.*, 2010, **5**, pp. 1490–1493
[4] Li Q., Fan S., Tang Z., Xing W.: 'Non-linear dynamics of an electrothermally excited resonant pressure sensor', *Sens. Actuators A, Phys.*, 2012, **188**, pp. 19–28
[5] Burns D.W., Zook J.D., Horning R.D., Herb W.R., Guckel H.: 'Sealed-cavity resonant microbeam pressure sensor', *Sens. Actuators A, Phys.*, 1995, **48**, pp. 179–186
[6] Welham C.J., Greenwood J., Bertioli M.M.: 'A high accuracy resonant pressure sensor by fusion bonding and trench etching', *Sens. Actuators A, Phys.*, 1999, **76**, (1–3), pp. 298–304
[7] Ikeda K., Kuwayama H., Kobayashi T., *ET AL.*: 'Silicon pressure sensor integrates resonant strain gauge on diaphragm', *Sens. Actuators A, Phys.*, 1990, **21**, (1–3), pp. 146–150
[8] Corman T., Enoksson P., Stemme G.: 'Low-pressure-encapsulated resonant structures with integrated electrodes for electrostatic excitation and capacitive detection', *Sens. Actuators A, Phys.*, 1998, **66**, (1–3), pp. 160–166
[9] Chuang W.-C., Lee H.-L., Chang P.-Z., *ET AL.*: 'Review on the modeling of electrostatic MEMS', *Sensors*, 2010, **10**, pp. 6149–6171
[10] Koumela A., Mercier D., Gouttenoire V., *ET AL.*: 'Silicon nanowire resonator with integrated electrostatic actuation', *Procedia Eng.*, 2011, **25**, pp. 1649–1652
[11] Kim Y., Choo S.-H.: 'Measurements of residual stress in the thin film micro-gas sensors containing metallic layers', *Thin Solid Films*, 2001, **394**, (1–2), pp. 283–290
[12] Matsumoto Y., Nishimura M., Matsuura M., Ishida M.: 'Three-axis SOI capacitive accelerometer with PLL C–V converter', *Sens. Actuators A, Phys.*, 1999, **75**, (1), pp. 77–85
[13] Mestrom R.M.C., Fey R.H.B., Phan K.L., Nijmeijer H.: 'Simulations and experiments of hardening and softening resonances in a clamped–clamped beam MEMS resonator', *Sens. Actuators A, Phys.*, 2010, **162**, (2), pp. 225–234

© The Institution of Engineering and Technology 2013